FORECASTING A GREAT BASIN CYCLOGENIC EVENT USING THE NESTED GRID MODEL: A CASE STUDY EVALUATION OF MODEL PERFORMANCE

Michael C. Conger

National Weather Service Forecast Office
Salt Lake City, Utah

Abstract

A late October 1989 storm associated with a rapidly intensifying 700-mb low over western Utah produced widespread heavy amounts of rain and snow across northwest Utah. A "conventional" examination of vertical motion forcing using Nested Grid Model (NGM) 500-mb positive vorticity advection (PVA) placed the strongest upward vertical motions well south of the area of cyclogenesis. Subjective analysis of rawinsonde data prior to and during the development of the storm indicates the greatest upward motions were further north and more closely related to the precipitation maximum. This evidence suggests that the NGM had trouble initializing the data fields.

In order to verify this possibility, gridded data fields generated from the NGM were examined using GEMPAK software. These fields consisted of the 00-hour and 12-hour forecasts prior to and the 00-hour forecast during the development of the storm. Two approaches were used to examine the model output. The first approach was a comparison of model output against the corresponding subjective analyses of 250-mb isotachs and 700-mb geopotential heights, winds and temperatures. The second approach was to generate difference fields (00-hour forecast minus the previous 12-hour forecast) for the 250-mb observed and ageostrophic winds, for the divergence of the observed and ageostrophic winds, and for cross sections of omega overlaid with the ageostrophic circulation tangent to the cross section at the exit region of the jet streak.

Results of this study show: 1) a "conventional" examination of vertical motion forcing using 500-mb PVA failed to explain heavy precipitation over northwest Utah; 2) the model's trouble in properly identifying the jet streak at 1200 UTC 25 October, led to a 12-hour forecast where the ageostrophic forcing of vertical motion and the attending secondary (indirect) circulation were much less than in the 00-hour forecast valid 0000 UTC 26 October; 3) that small differences between the 00-hour and 12-hour forecast fields of the total wind both valid at 0000 UTC 26 October produced large differences in the total ageostrophic wind; and, 4) the model's difficulty in representing the 700-mb wind and generation of a closed circulation center over eastern Nevada.

1. Introduction

Between 1800 UTC 25 October 1989 and 1800 UTC 26 October 1989, widespread heavy precipitation amounts were recorded across northwest Utah. A cold-core, 700-mb low moving southeast across Nevada on the afternoon of the 25th experienced rapid intensification as it entered western Utah during the local afternoon hours. Thunderstorms developed over western Utah along the strong baroclinic zone associated with the 700-mb low and continued until around 0300 UTC. After 0600 UTC on the 26th, the 700-mb low accelerated northeastward through central Utah. The main area of precipitation shifted to northern Utah with the heaviest amounts confined to the northwest quarter of the state. By 1500 UTC on the 26th, the storm center had moved into southwest Wyoming with precipitation ending over all but northeast Utah around 1800 UTC.

Climatologically, heavy precipitation events (≥25 mm/24 hours) in Utah are rare. When they occur, they are commonly associated with strong convection or orographic enhancement. In either event, heavy precipitation is generally confined to a limited geographic area. The 25–26 October storm was exceptional in that heavy precipitation was not localized, but spread over a relatively large area of the northwest valleys and mountains (Fig. 1).

Typically, a moist, cold-core, 700-mb low moving through the Great Basin will produce widespread light precipitation without any significant intensification of the low. In this storm, however, the 700-mb low intensified over the Great Basin during the afternoon of the 25th. The resultant enhanced upward vertical motion supported strong convective activity and heavy precipitation over western Utah. As the 700-mb low moved northeast through Utah early on the 26th, the flow over northwest Utah gradually backed to a northwesterly direction. The resultant cold air advection across the Great Salt Lake triggered "lake-effect" precipitation in the lee of the lake and amplified orographically induced snowfalls in the mountains Carpenter (1985).

From a forecaster's perspective, it was not readily apparent from the National Weather Service (NWS), National Meteorological Center's Nested Grid Model (NGM) output that the greatest upward vertical motion would be over western Utah on the afternoon of the 25th. A "conventional" estimation of vertical motion, as described by Dunn (1988), using 500-mb positive vorticity advection (PVA) from the 1200 UTC 25 October, NGM (00-hour and 12-hour forecasts) placed the greatest upward vertical motions over western Arizona/ extreme southern Utah by 0000 UTC 26 October (Fig. 2). Vertical motion (omega) at 700 mb from the same NGM cycle did support stronger upward vertical motions over western Utah in the 12-hour forecast (Fig. 3a). However, omega from the NGM 00-hour forecast valid 0000 UTC 26 October, placed the strongest upward vertical motions over northwest Arizona (Fig. 3b) even though 700-mb cyclogenesis and heavy convective precipitation were taking place over western Utah.

In this study, the trouble that the model has properly locating vertical motion forcing associated with 700-mb cyclogenesis will be examined primarily from an ageostrophic perspective. Subjective analysis of rawinsonde/airep data will be compared against corresponding NGM output (both 00-hour and 12-hour forecasts). Normally, the Salt Lake City, NWS Forecast Office uses the 250-mb and 700-mb pressure surfaces to represent the jet and lower levels of the atmosphere, respectively. This convention will be followed in this paper. Discrepancies found between observed data and the

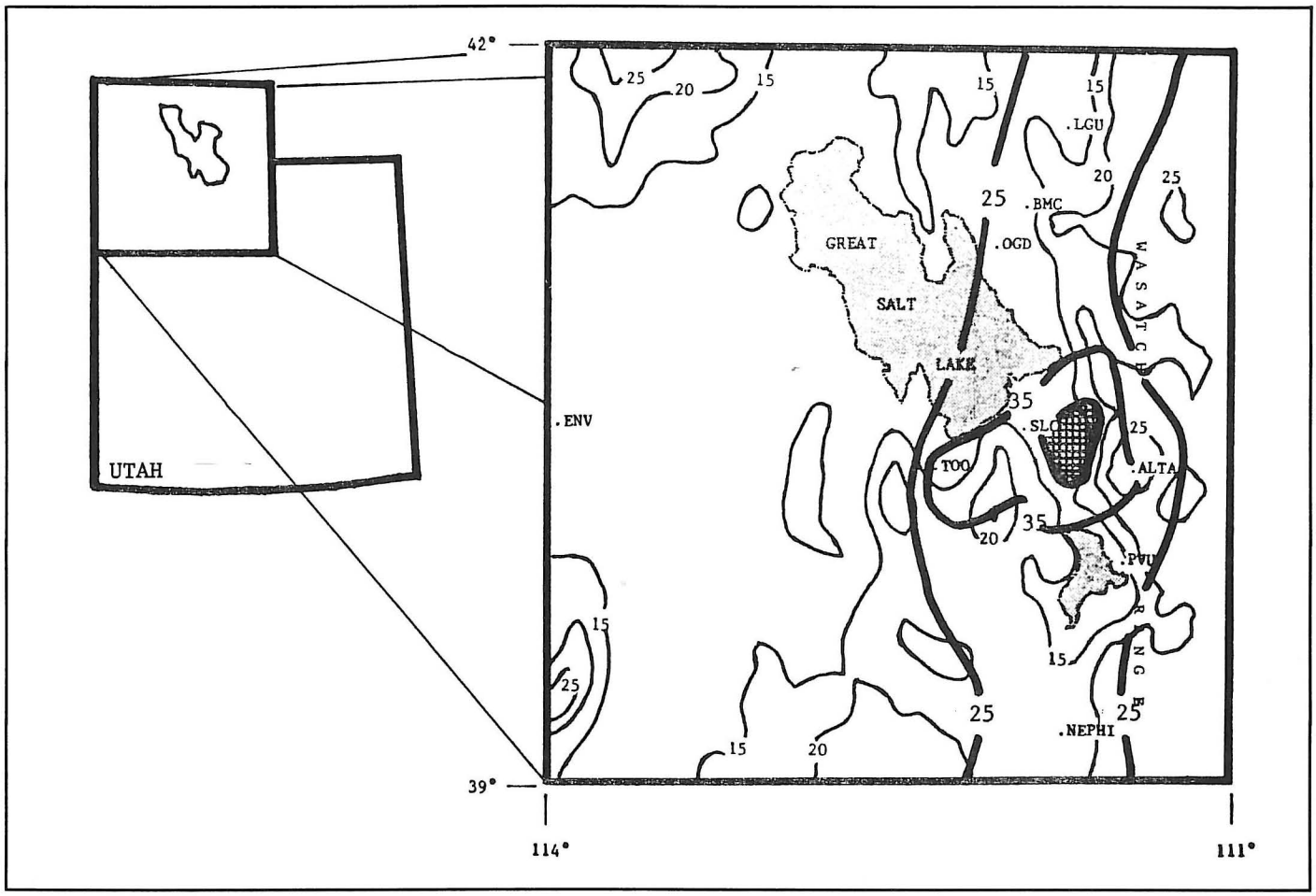

Fig. 1. Distribution of heavy 24-hour precipitation over northern Utah from 1800 UTC 25 October to 1800 UTC 26 October 1989. Precipitation isopleth (solid, thick) intervals 10 mm above 25 mm. Gridded region ≥ 45 mm. Elevation isopleth (solid, thin) intervals 500 m above 1500 m.

corresponding 00-hour forecasts will be identified and offered as a means of explaining why the model failed to forecast the proper location and intensity of this storm.

Using the gridded data from the NGM and GEMPAK software developed at the NWS/National Meteorological Center (NMC) by desJardin et al. (1988) to produce the graphical output, the improper initialization of the jet streak will be documented. Difference fields at the 250-mb level(0000 UTC 26 October, 00-hour forecast minus 1200 UTC 25 October, 12-hour forecast) for wind (total and ageostrophic) and divergence of the ageostrophic wind will be computed along with a difference cross-section of the ageostrophic circulation and vertical motion (omega) tangent to the cross-section through the exit region of the jet streak. These computed fields will serve to quantify the model's problem in handling the jet streak and the subsequent failure to handle the attending secondary circulation.

2. Comparisons of Subjective Analysis Against Corresponding NGM Output

The NGM is the forecast portion of the NWS/NMC Regional Analysis and Forecast System (RAFS). It is a 16-layer, hemispheric, primitive equation model utilizing two-way interactive nested grids. Three nested grids (A, B, and C) are utilized by the NGM with the highest resolution in the C-grid (resolution 84 km at 45°N) which is centered over North America. A number of physical processes are involved in the NGM. A thorough discussion of these processes and other facets of the NGM are given in Carr (1988) and Hoke et al. (1989). Significant changes have occurred in the NGM and RAFS since their inception (March 1985) until the time of this study (October 1989). Discussions of these changes can be found in Bonner and Petersen (1989) and Parish (1989). The NGM gridded data obtained from NMC was interpolated to the Limited area Fine Mesh (LFM) grid (190.5 km at 60°N) for archiving rather than on the original NGM C-grid.

In an operational forecast environment, the first step in determining the reliability of the model output is to compare the 00-hour forecast fields (sometimes referred to as the initial analysis in the operational environment) against observed data (rawinsonde/airep, surface observations, satellite imagery, etc.). Here discrepancies in model output can be identified and their impact on the model's forecast (e.g., storm development/decay, temperatures/wind fields, etc.) assessed.

At 1200 UTC 25 October, 250-mb isotachs produced through a subjective analysis of rawinsonde/airep data were

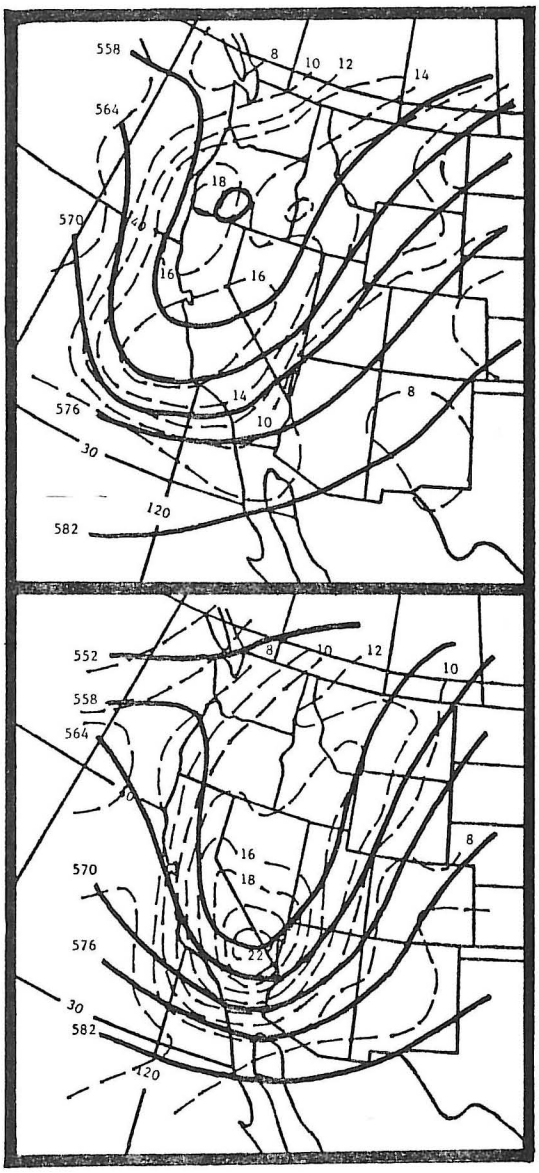

Fig. 2. NGM 500-mb geopotential height (solid, intervals 6 dm) and vorticity (dashed, intervals $2x10^{-5}$ s^{-1}) from 1200 UTC 25 October (a) 00-hour forecast and (b) 12-hour forecast valid at 0000 UTC.

Fig. 3. NGM 700-mb omega valid 0000 UTC 26 October from (a) 1200 UTC 25 October, 12-hour forecast and (b) 00-hour forecast. Intervals are 2 μb s^{-1}.

compared against NGM output prior to rapid cyclogenesis over western Utah. Both methods showed the jet stream off the southern California coast then arcing northeast into the Great Basin and continuing into southern Canada (Fig. 4). Within the jet stream, two 55m s^{-1} jet streaks were identified in the subjective analysis; one over southern California and the other over northeast Nevada/northwest Utah. In the NGM output, there is a suggestion of these features, though core speeds were slightly less than those observed.

At 0000 UTC 26 October, the subjective analysis of rawinsonde /airep data and the NGM 00-hour forecast both placed the jet stream from southern California northward into southern Canada (Figs. 5a&b). Two separate jet streaks were identified with the one affecting Utah extending from southwest Arizona into northeast Utah/northwest Colorado. As was the case at 1200 UTC 25 October, the 0000 UTC 26 October, NGM 00-hour forecast (Fig. 5b) produced core wind speeds slightly less than the maximum observed wind speed from the rawinsonde data (Fig. 5a). Interestingly, the 12-hour forecast valid at 0000 UTC 26 October, (Fig. 5c) did forecast winds of 50m s^{-1} or greater through eastern Utah, though the core of strongest winds extends much further southwest than the observed winds indicate.

Though the emphasis of this study is on the jet streak-induced vertical motions, discrepancies found between observed and 700-mb NGM forecast data of temperature, geopotential height and wind warrant discussion. Prior to rapid cyclogenesis (1200 UTC 25 October), few differences were noted between the observed and 00-hour forecast temperatures across Nevada (Figs. 6a&b). By 0000 UTC 26 October, the 12-hour forecast valid at 0000 UTC (Fig. 6c) had temperatures as much as 4°C warmer than observed

Fig. 4. 1200 UTC 25 October, 250-mb isotachs produced from (a) subjective analysis of rawinsonde/airep data and (b) NGM 00-hour forecast. Intervals are 10 m s^{-1} above 35 m s^{-1}. Dashed areas ≥ 55 m s^{-1}.

(Fig. 6d) over eastern Nevada. The 00-hour forecast valid at 0000 UTC showed little improvement as temperatures remained as high as 3°C warmer than observed across western Utah/eastern Nevada (Fig. 6e).

Subtle, yet important differences were detected in comparisons of the 700-mb geopotential height and winds. At 1200 UTC 25 October, both the subjective analysis and the NGM output of the geopotential heights show a trough through Nevada (Figs. 7a&c) with a weak circulation center evident in both the rawinsonde data and NGM output over extreme northern Nevada (Figs. 7a&b). By 0000 UTC, the subjective analysis placed a closed circulation center over western Utah (Fig. 8). This location was supported by satellite imagery (not shown). Neither the NGM 00-hour nor the 12-hour forecasts of geopotential height valid at 0000 UTC could identify this feature over western Utah (Figs. 9a&c). Instead, circulation centers were defined in the wind field much further north over southwest Montana and central Idaho, respectively (Figs. 9b&d).

Evidence presented has shown that certain elements of observed wind, temperature and geopotential height differ from those represented in the NGM gridded data fields (both the 00-hour and 12-hour forecasts valid 0000 UTC 26 October). Arguments will be presented to show from an ageostrophic perspective that although the 00-hour and 12-hour forecasts of the total wind valid at 0000 UTC appear similar, minor variations between them result in large differences in the amount of ageostrophic forcing each indicates.

3. NGM Forecast Difficulty in Handling the Jet Streak: An Ageostrophic Perspective

According to Bjerknes (1951), Uccellini and Johnson (1979), Murray and Daniels (1953), Namias and Clapp (1949) and others, a jet streak with little or no curvature at the entrance region has a transverse ageostrophic component directed toward the cyclonic-shear (left-rear) side of the jet. Conversely, at the exit region the ageostrophic component is directed toward the anticyclonic-shear (right-front) side of the jet (Fig. 10). At the entrance region, this ageostrophic component represents the upper branch of the direct circulation. This circulation is marked by rising (sinking) motion on the anticyclonic or warm (cyclonic or cold) side of the jet. At the exit region, this component represents the upper branch of the indirect circulation with the rising (sinking) motion on the cyclonic or cold (anticyclonic or warm) side of the jet.

Prior to this study, the National Weather Service Forecast Office (NWSFO) at Salt Lake City received most of their diagnostic and prognostic information through the Automation of Field Operations and Services (AFOS) system. Data on ageostrophic parameters were not available from the NGM (or any other model) on AFOS. Personal computer (PC) based diagnostics developed by Foster (1988) were available using mandatory pressure levels for the base data. However, this software did not output ageostrophic parameters.

Without objectively produced ageostrophic data, forecasters must rely on the conceptual four quadrant straight-line jet streak to identify areas of vertical motion. This method, while generally effective, makes certain assumptions which are not always correct (i.e., the stronger the jet streak the greater the vertical motions, upward vertical motions always occur in the left-front/right-rear quadrants of the jet streak) and neglect the effects that thermal structure and orientation (curvature) have on vertical circulations (motions). Later in this study it will be shown that two jet streaks of similar magnitudes, but slightly different orientations, can result in substantial differences to the ageostrophic component of the wind.

With the 250-mb trough just upstream from the jet streak, strong curvature exists at the entrance region of the jet streak. A study by Cammas and Ramond (1989) demonstrated that the effects of curvature can be predominant to the point that the direct circulation is masked in the upper tropospheric divergence field. In this storm, the greatest development occurred in the exit region of the jet where curvature effects were minimal. It will be shown that an indirect circulation does exist at the exit region of the jet streak similar to what is defined in the straight-line jet streak.

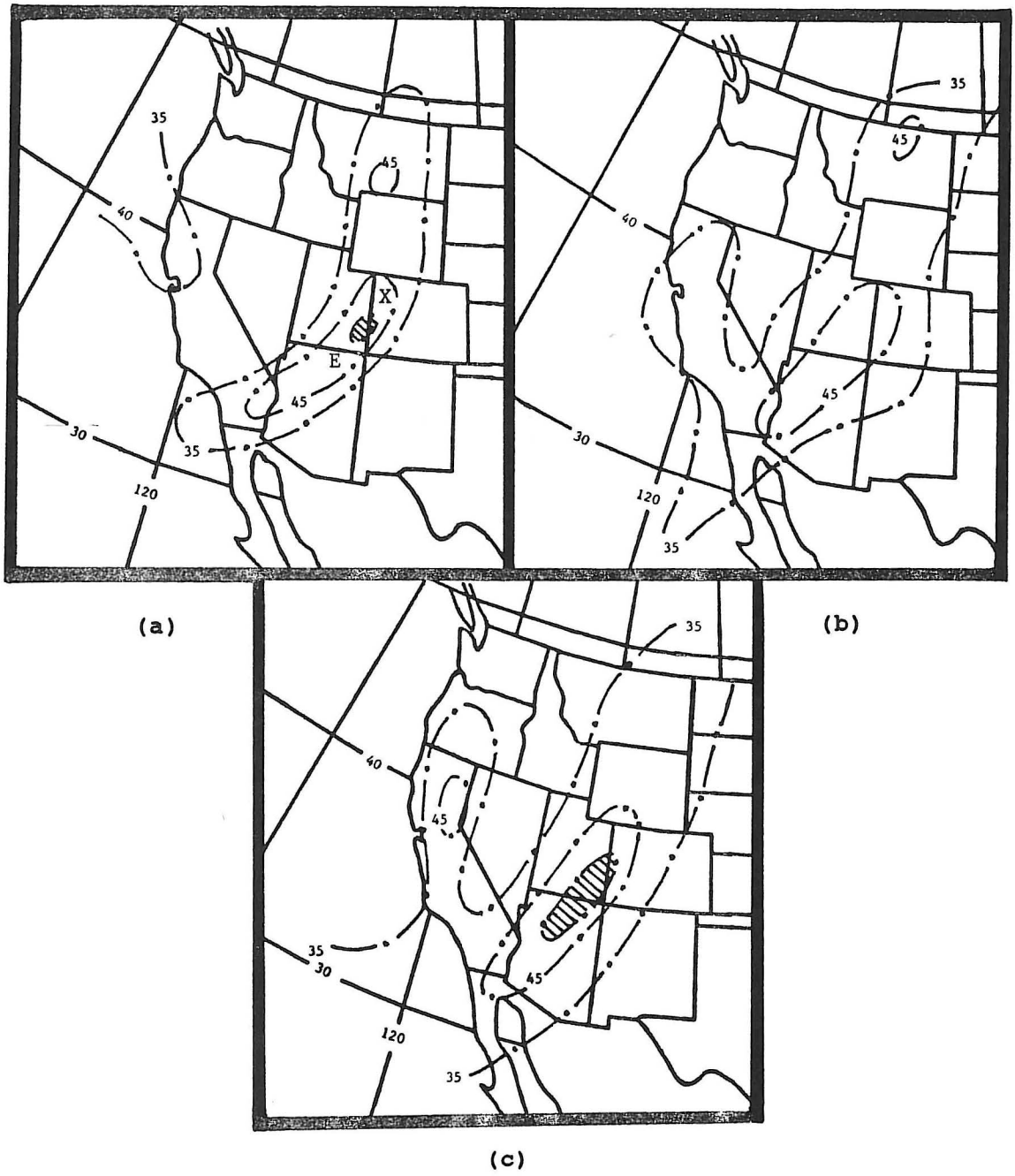

Fig. 5. 0000 UTC 26 October, 250-mb isotachs from (a) analysis of rawinsonde/airep data, (b) NGM 00-hour forecast and (c) 1200 UTC 25 October, 12-hour forecast valid at 0000 UTC. Intervals are 10 m s^{-1} above 35 m s^{-1}. Dashed areas $\geq$ 55 m s^{-1}. Entrance and exit regions of the jet streak in (a) represented by E and X respectively.

To quantify the NGM's handling of the jet streak, difference fields at the 250-mb level (00-hour forecast minus the 12-hour forecast valid at 0000 UTC) for the total and ageostrophic winds were computed. The isotachs of the total wind for the 00-hour and 12-hour forecasts (Figs. 11a&b respectively) valid 0000 UTC appear quite similar. The only notable difference is more elongation of the jet streak in the 12-hour forecast. The magnitude of the difference (Fig. 11c) was quite small with the 00-hour forecast values ranging from 1–4 m s^{-1} slower than the 12-hour forecast across northern Arizona, Utah and western Colorado.

Though the magnitude of the differences were small, they did produce substantial differences in the magnitude of the ageostrophic wind. Comparisons of the 00-hour and 12-hour forecasts of the ageostrophic wind (Figs. 12a&b respectively) both show the strongest ageostrophic winds through the base of the trough at the entrance region of the jet. The core of the strongest ageostrophic winds extends further north and east in the 00-hour forecast. Also, within the exit region of the jet, the magnitudes of the 00-hour forecast are stronger than in the 12-hour forecast.

Examination of the difference field for the ageostrophic

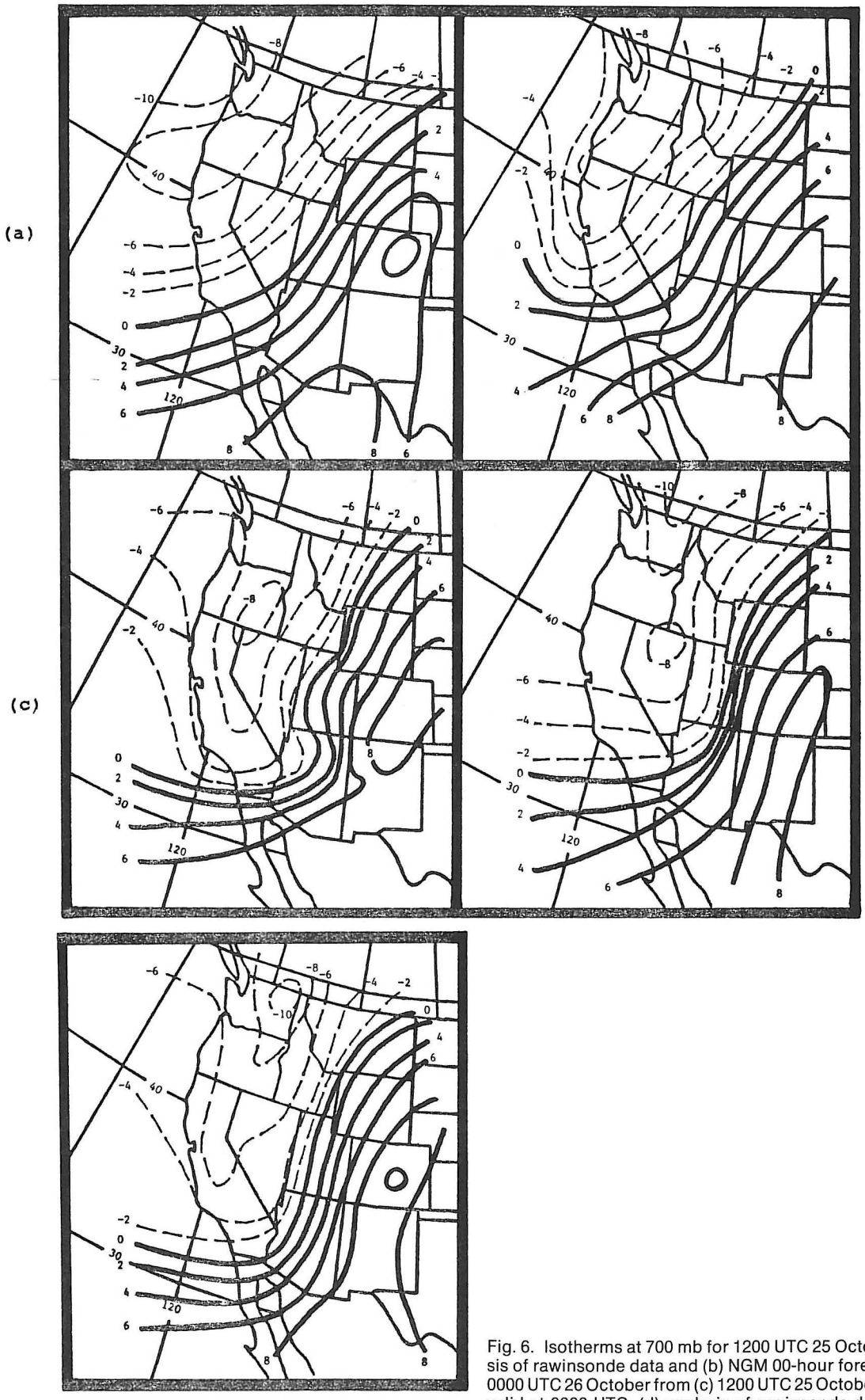

Fig. 6. Isotherms at 700 mb for 1200 UTC 25 October from (a) analysis of rawinsonde data and (b) NGM 00-hour forecast. Isotherms for 0000 UTC 26 October from (c) 1200 UTC 25 October, 12-hour forecast valid at 0000 UTC, (d) analysis of rawinsonde data and (e) 00-hour forecast. Intervals are 2°C.

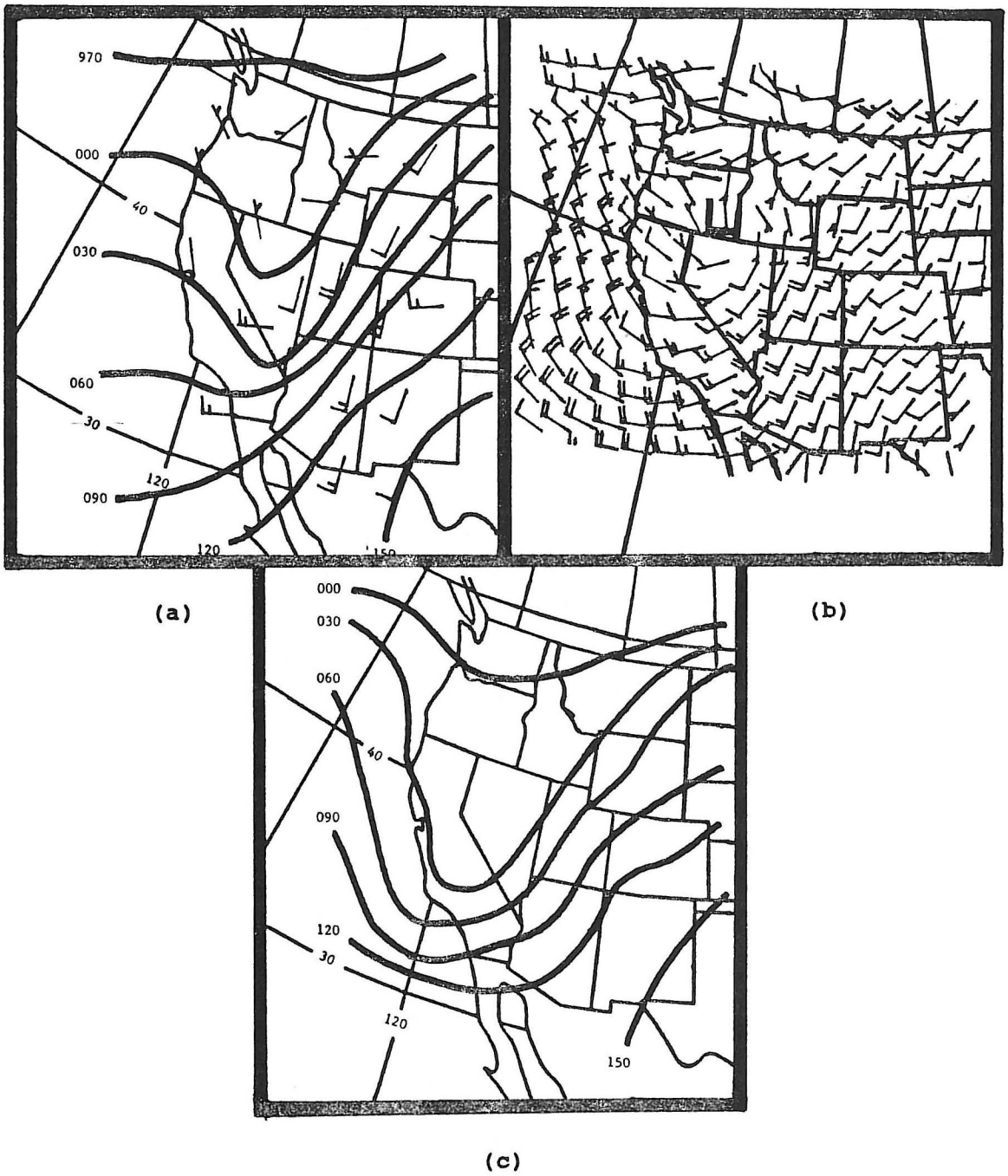

Fig. 7. 1200 UTC 25 October, 700-mb (a) analysis of heights and winds from rawinsonde data, (b) NGM 00-hour forecast of winds and (c) NGM 00-hour forecast of geopotential heights. Height intervals are 30 m centered on 3000 m.

wind illustrates these differences quite well. Underforecasting of the magnitude approaches 7 m s^{-1} near the entrance region of the jet, while at the exit region it approaches 10 m s^{-1} (Fig. 12c). When the ageostrophic wind is broken down into it's longitudinal (along stream) and transverse (cross stream) components (Figs. 13a&b), the difference in the total ageostrophic wind at the entrance region of the jet appears to result from a stronger longitudinal component in the 00-hour forecast. At the exit region of the jet, the transverse component in the 00-hour forecast appears stronger than in the 12-hour forecast through western Colorado. This stronger transverse component in the 00-hour forecast could indicate that a stronger secondary (indirect) circulation exists at the exit region of the jet streak than was previously forecast.

The seemingly minor differences in the total wind speed within the jet stream were demonstrated to have a profound impact on the total (longitudinal and transverse) ageostrophic motion which in turn affects the convergence/divergence pattern associated with jet dynamics. Further evidence of this impact can be gathered by examining the divergence of the

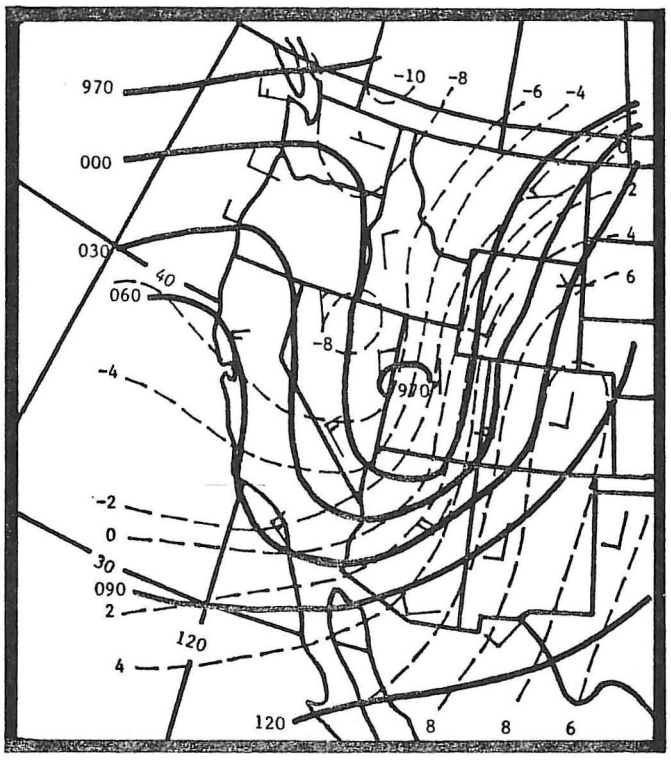

Fig. 8. Subjective analysis from 700-mb rawinsonde data of geopotential height (solid), temperature (dashed) and wind (barbs) for 0000 UTC October 26. Height intervals are 30 m centered on 3000 m. Temperature intervals are 2°C

ageostrophic wind. On a constant pressure surface, the ageostrophic divergence is expressed as:

$$\nabla_p \cdot V_a = \nabla_p \cdot V - \nabla_p \cdot V_g \qquad (1)$$

where V_a is the ageostrophic wind and V_g is the geostrophic wind. Through scaling arguments, both the ageostrophic divergence and total divergence maximum are approximately an order of magnitude higher than the geostrophic divergence maximum. Therefore, the divergence of the ageostrophic wind can be used to interpret the divergence/convergence maximum of the total wind by neglecting the lesser ordered first approximation of the geostrophic divergence. In this case, the maximum divergence of the ageostrophic wind from the 00-hour forecast was centered over southern Utah (Fig. 14a) while in the 12-hour forecast (Fig. 14b) a weaker divergence maximum was placed over northwest Arizona. The resultant difference field has a stronger than forecast divergence maximum on the order of 2 x 10^{-5} s^{-1} located near the exit region of the jet streak (Fig. 14c).

Evidence presented so far has shown in a two-dimensional sense how the transverse circulations were affected by differences in the forecast of the total wind. However, indirect (and direct) circulations are a consequence of three-dimensional variations in the ageostrophic wind and upper-level divergence that a two-dimensional straight-line jet streak does not adequately explain (Uccellini et al. 1984, Keyser and Shapiro 1986, Newton and Trevisan 1984; and others).

To illustrate this point and to show how the model mishandled the indirect circulation, cross-sections of the ageostrophic wind and omega were computed through the exit region of the jet streak. In both the 00-hour and 12-hour forecasts valid at 0000 UTC (Figs. 15a&b respectively), the indirect transverse circulation is definable. A subjective comparison of the two circulations shows that the upward branch of the circulation in the 00-hour forecast appears stronger and further east than in the 12-hour forecast. A difference cross-section (Fig. 15c) confirms that the 00-hour forecast does in fact have the stronger circulation.

The NGM's inability to properly identify the jet streak has led to considerable underdevelopment of the three-dimensional vertical circulation associated with the exit region of the jet streak. The extent that this underforecasting affected precipitation over northern Utah is not quantitatively definable in this study. However, when viewed from a strictly upper tropospheric dynamics perspective, the vertical motion indicated in the 12-hour forecast was probably not strong enough to support the deep convection observed early in the storm across western Utah (this neglecting the diabatic effects that may have played heavily at this point to enhance vertical motions induced by the jet streak).

4. Summary

The rapid intensification of this late October storm implies that stronger vertical motion forcing existed than was indicated by the NGM output. A conventional examination of vertical motions using 500-mb pattern recognition placed the strongest vertical motions well south of where it was observed over western Utah.

An examination of vertical motion forcing from a strictly ageostrophic perspective was done using both observed data and NGM gridded data fields for comparison. Subjective analysis of observed rawinsonde/airep data prior to development of the storm defined a jet streak configuration that the NGM 00-hour forecast smoothed and weakened slightly. This would imply that jet streak-induced vertical motions, as viewed in terms of a straight-line jet streak, in the left-front quadrant of the observed jet streak were stronger than those in the model's jet streak. This supports the rapid intensification observed as the low entered western Utah and may explain why the model did not forecast the intensity or location of this event. The failure to properly place the jet further east in the 12-hour forecast was also illustrated in the difference fields of total and ageostrophic winds. The model's 12-hour forecast of the total wind, while similar to the 00-hour forecast total wind valid the same time, failed to identify a well defined jet streak. This resulted in a weaker ageostrophic flow which would indicate that less vertical motion forcing existed in the exit region of the jet streak. The affect on the attendant secondary (indirect) circulation at the exit region of the jet streak was that a much weaker vertical circulation exists in the 12-hour forecast than in the 00-hour forecast valid 0000 UTC.

Interestingly, the difference in magnitude between the model's forecasted wind speeds (00-hour and 12-hour) only varied by a few m s^{-1} through the jet streak. However, the magnitude of the ageostrophic wind was considerably larger in the 00-hour forecast even though the wind speeds were slightly higher in the 12-hour forecast. This illustrates that it's not the magnitude of the wind velocity within the jet streak, but variations in the longitudinal and transverse components of the total wind that influences vertical motion.

Discrepancies found in comparisons of NGM gridded data (00-hour and 12-hour forecasts) against observed data (temperature, wind, and geopotential height) at the 700-mb level

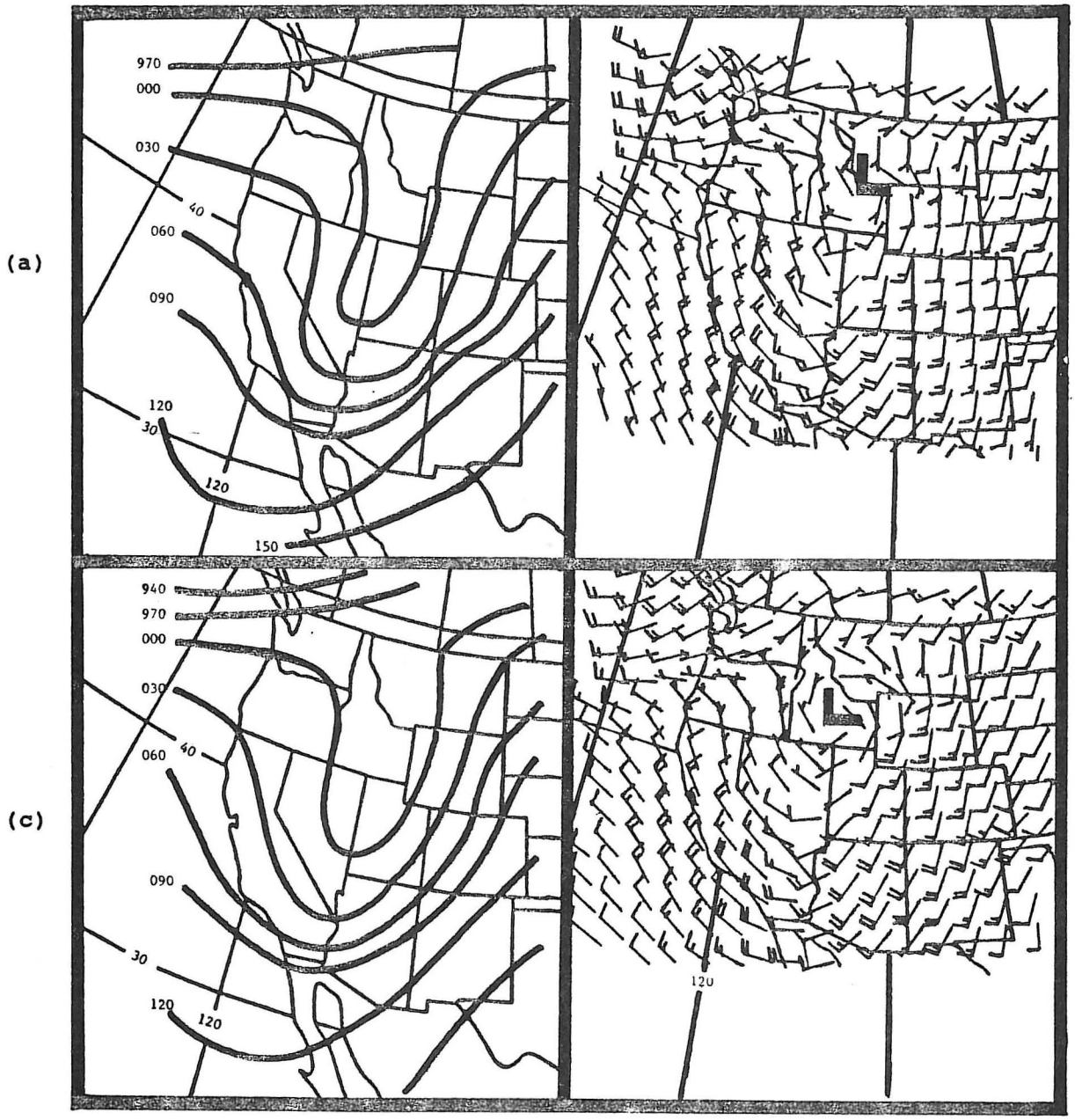

Fig. 9. NGM 700-mb 00-hour forecasts valid 0000 UTC 26 October, for (a) geopotential heights and (b) wind. Fig. 9 (c) & (d) same as (a) & (b) respectively for 1200 UTC 25 October, 12-hour forecasts valid at 0000 UTC. Height intervals are 30 m centered on 3000 m.

further illustrates the model's difficulty in forecasting this storm. Considerable differences between observed and forecast winds were found in the NGM output. Both the 00-hour and 12-hour forecasts of the wind valid at 0000 UTC placed a circulation center well north of where it was actually located in the observed data. Model output of the geopotential heights also performed poorly in identifying the 700-mb low center. Though the actual geopotential height values from the model were close to the observed values (consistently 10–20 m higher than the observed values), they failed to indicate a closed circulation apparent in the observed wind data and supported by satellite imagery. Differences in the temperature from the model output ranged from 1–4°C warmer than observed through western Utah/eastern Nevada during peak cyclogenesis. The influence these differences had on diabatic effects (especially latent heat release) were not examined in this study. However, in a study by Keyser and Johnson (1984), diabatic effects were found to intensify a jet streak-induced vertical circulation. Considering the explosive nature of this storm's development and the deep convection observed, it's conceivable that diabatic effects did play heavily in this particular storm.

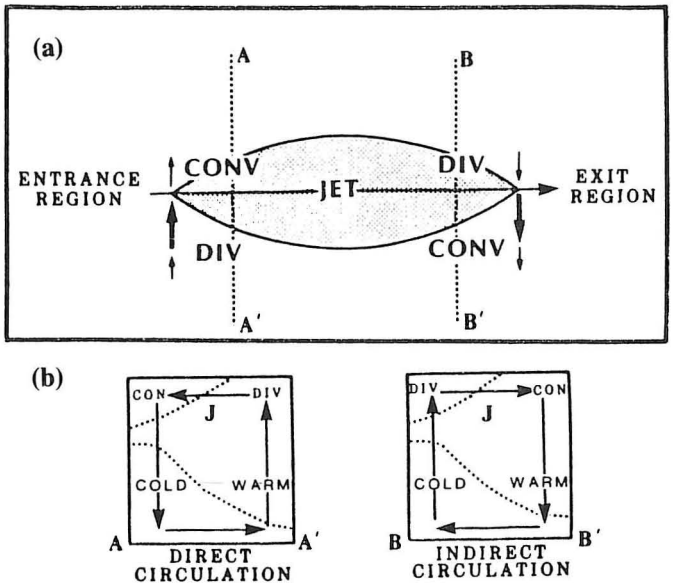

Fig. 10. (a) Schematic of transverse ageostrophic wind components and patterns of divergence associated with the entrance and exit regions of a straight jet streak (after Bjerknes 1951) and (b) vertical cross sections illustrating direct and indirect circulations in the entrance region (along line A-A') and exit region (along line B-B') of a jet streak.

5. Conclusions

Within the operational forecasting environment, two important points can be gained from this study. One, subjective analysis of observed data provides a means of identifying areas of vertical motion forcing and verifying the accuracy of the model's 00-hour forecasts. Two, vertical motion results from a number of physical and three-dimensional processes and is not simply confined to conventional 500-mb parameters. With the coming of gridded data, the meteorologist (forecaster) will have to become familiar with the theory behind vertical motion forcing in order to effectively use the new data that is becoming available in the modernized National Weather Service Forecast Offices and elsewhere.

Acknowledgments

I would like to thank Louis W. Uccellini and his NMC Meteorological Operations Division staff for their help with this study and for the time spent at NMC. Also, thanks to Tim Barker and Larry Dunn of the NWS Western Region Headquarters, Scientific Services Division for their help.

Author

Michael Conger is currently a Lead Forecaster at the National Weather Service Forecast Office (NWSFO) in Salt Lake City, Utah. After an internship with the NWSFO at Boise, Idaho, Mr. Conger transferred to Salt Lake City in 1987 as a Journeyman Forecaster with a promotion to Lead Forecaster in 1990. He attended Iowa State University where he earned a B.S. degree in Meteorology in 1981. He then earned a M.S. degree at the University of Utah in 1989.

References

Bjerknes, J., 1951: Extratropical cyclones. *Compendium of Meteorology,* T. F. Malone, Ed., Amer. Meteor. Soc., 577–598.

Bonner, W. D., and R. A. Petersen, 1989: Recent changes to NMC's analysis and forecast systems. *Wea. Forecasting,* 4, 81–82.

Cammas, J-P, and D. Ramond, 1989: Analysis and diagnosis of the composition of ageostrophic circulations in jet-front systems, *Mon. Wea. Rev.*, 117, 2447–2461.

Carpenter, D. M. 1985: Great Salt Lake effect snowfall: some notes and an example. *NOAA Technical Memorandum NWS WR-190,* NWS Western Region, Salt Lake City, UT.

Carr, F. H., 1988: *Introduction to numerical weather prediction models at the National Meteorological Center.* NOAA National Weather Service Southern Region, Ft. Worth, TX, 63 pp.

desJardins, M. L., K. F. Brill, and S. S. Schotz, 1988: Gempak5, *NASA Tech. Mem. 4260,* V5.

Dunn, L. B., 1988: Vertical motion evaluation of a Colorado snowstorm from a synoptician's perspective. *Wea. Forecasting,* 3, 261–272.

Foster, M. P., 1988: UA Diagnostics, Southern Region National Weather Service Computer Program. NWS Southern Region, Ft. Worth, TX.

Hoke, J. E., N. A. Phillips, G. J. DiMego, and J. G. Sela, 1989: The regional analysis and forecast system of the National Meteorological Center. *Wea. Forecasting,* 4, 323–334.

Keyser, D. A., and D. R. Johnson, 1984: Effects of diabatic heating on the ageostrophic circulation of an upper tropospheric jet streak. *Mon. Wea. Rev.*, 112, 1709–1724.

_____, and M. A. Shapiro, 1986: A review of the structure and dynamics of upper-level frontal zones. *Mon. Wea. Rev.*, 114, 452–499.

Murray, R., and S. M. Daniels, 1953: Transverse flow at entrance and exit to jet streams. *Quart. J. Roy. Meteor. Soc.*, 79, 236–241.

Namias, J., and P. F. Clapp, 1949: Confluence theory of the high tropospheric jet stream. *J. Meteor.*, 6, 330–336.

Newton, C. W., and A. Trevisan, 1984: Clinogenesis and frontogenesis in jet stream waves. Part I: Analytic relations to wave structure. *J. Atmos. Sci.*, 41, 2717-2734.

Parish, D. F., 1989: Applications of implicit normal mode initialization to the NMC nested grid model, *NMC office note No. 349,* National Meteorological Center, National Weather Service (NOAA), Camp Springs, Maryland, pp 33.

Uccellini, L. W., P. J. Kocin, R. A. Petersen, C. H. Wash and K. F. Brill, 1984: The Presidents' Day cyclone of 18–19 February 1979: Synoptic overview and analysis of the subtropical jet streak influencing the precyclogenetic period. *Mon. Wea. Rev.*, 112, 31–35.

_____, and D. R. Johnson, 1979: The coupling of upper- and lower-tropospheric jet streaks and implications for the development of severe convective storms. *Mon. Wea. Rev.*, 107, 682–703.

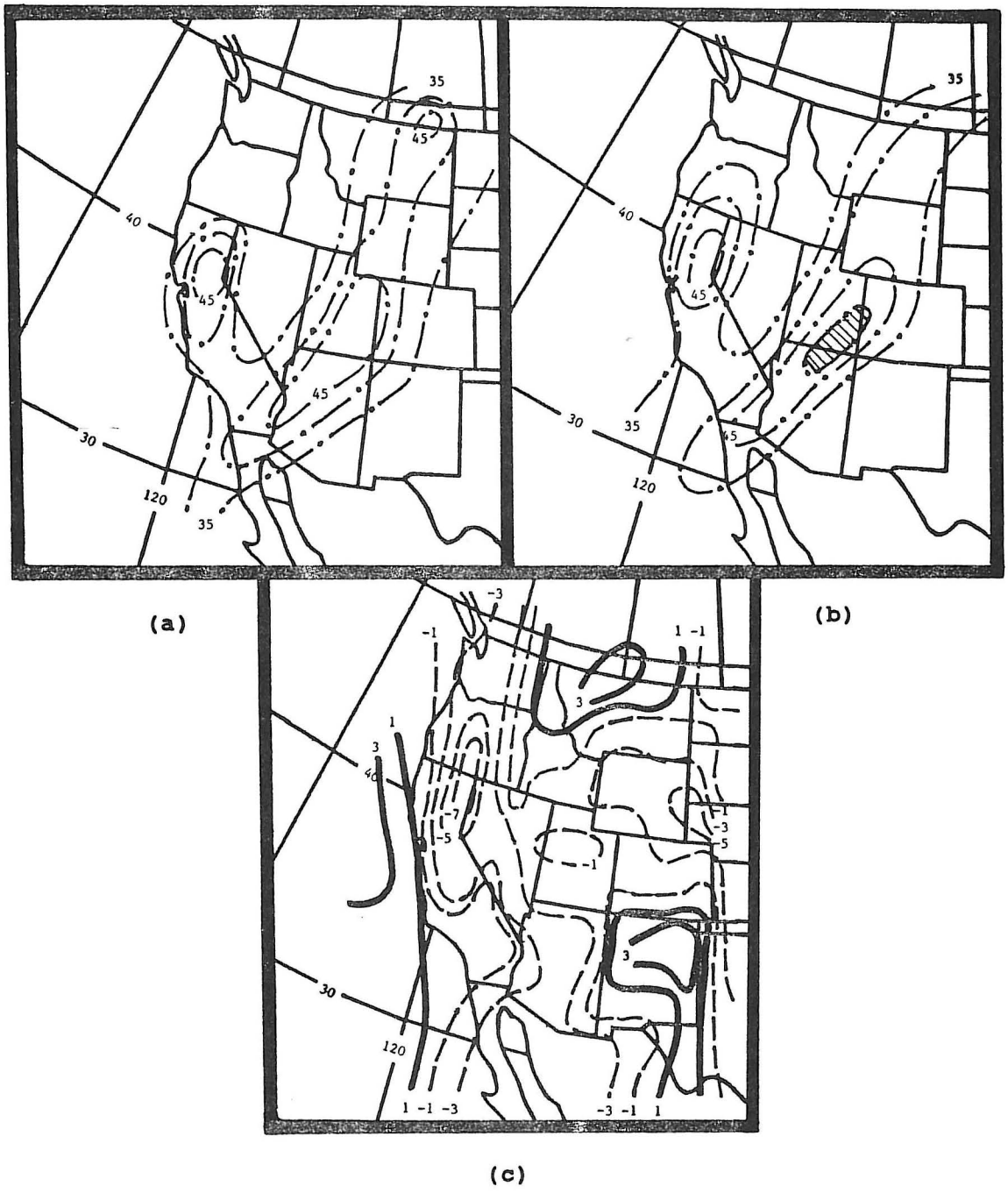

Fig. 11. NGM 250-mb isotachs valid at 0000 UTC 26 October for (a) 00-hour forecast and (b) 1200 UTC 25 October, 12-hour forecast, and (c) difference field of the total wind (00-hour minus 12-hour forecast). Intervals in (a) & (b) are 5 m s^{-1} beginning at 35 m s^{-1}. Dashed region ≥50 m s^{-1}.

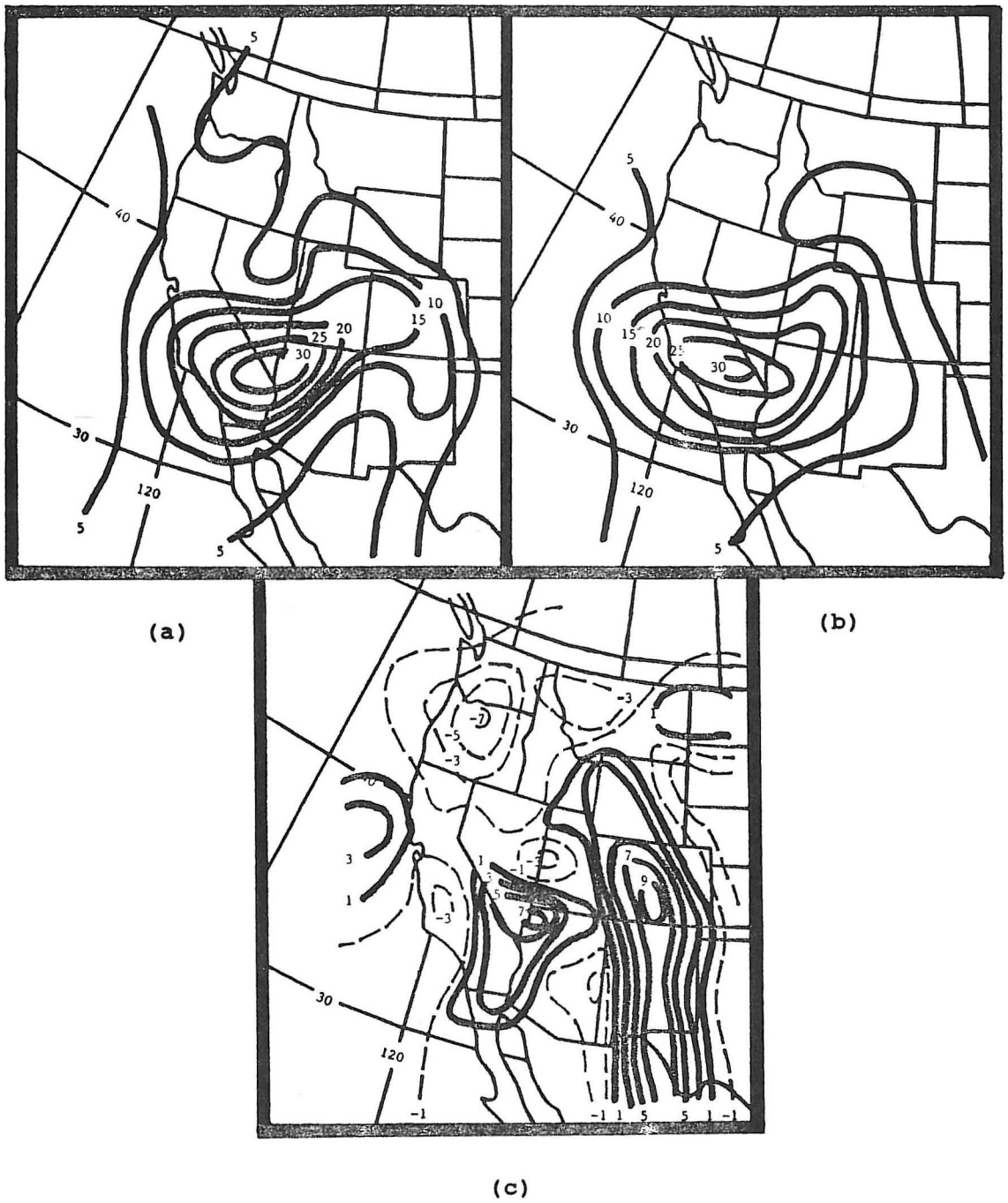

Fig. 12. NGM 250-mb ageostrophic winds valid at 0000 UTC 26 October for (a) 00-hour forecast and (b) 1200 UTC 25 October, 12-hour forecast, and (c) difference field of the ageostrophic wind (00-hour minus 12-hour forecast). Intervals in (a) & (b) are 5 m s^{-1} and in (c) 2 m s^{-1}.

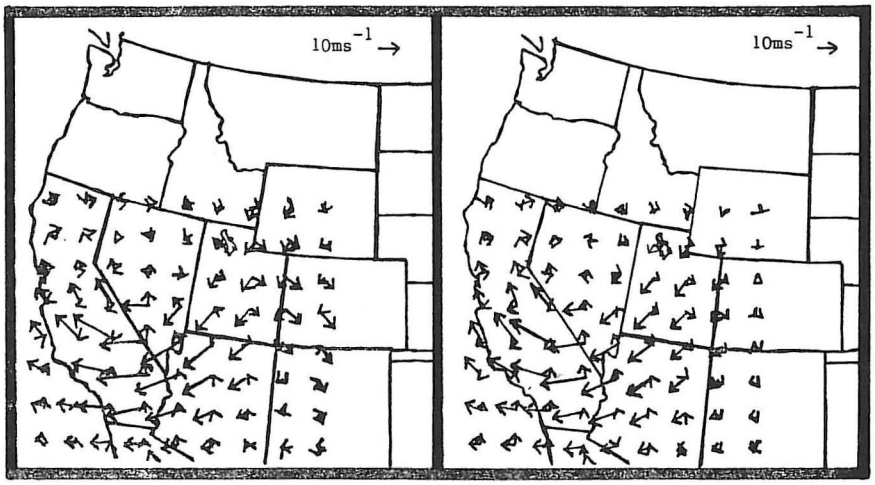

Fig. 13. Longitudinal and transverse components of the total ageostrophic wind valid at 0000 UTC 26 October for (a) 00-hour forecast and (b) 1200 UTC 25 October, 12-hour forecast.

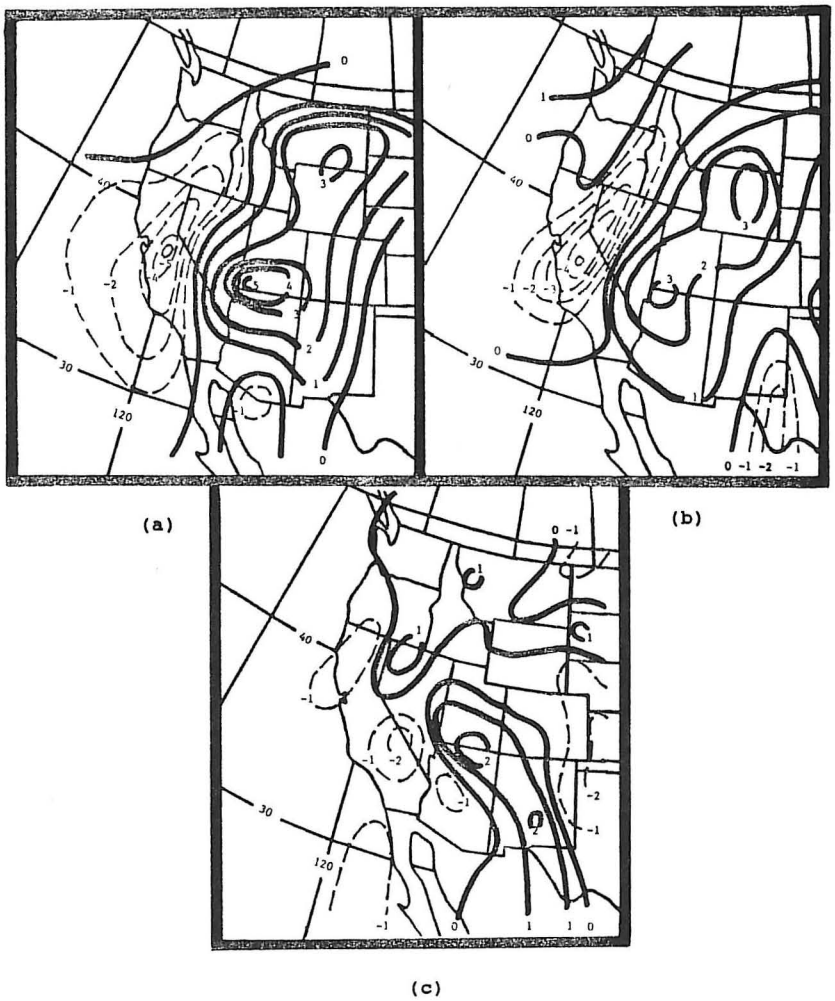

Fig. 14. Divergence of the ageostrophic wind valid at 0000 UTC 26 October for (a) 00-hour forecast and (b) 1200 UTC 25 October, 12-hour forecast, and (c) divergence of the difference of the ageostrophic wind (00-hour minus 12-hour forecast). Intervals are 1 x 10^{-5} s^{-1}.

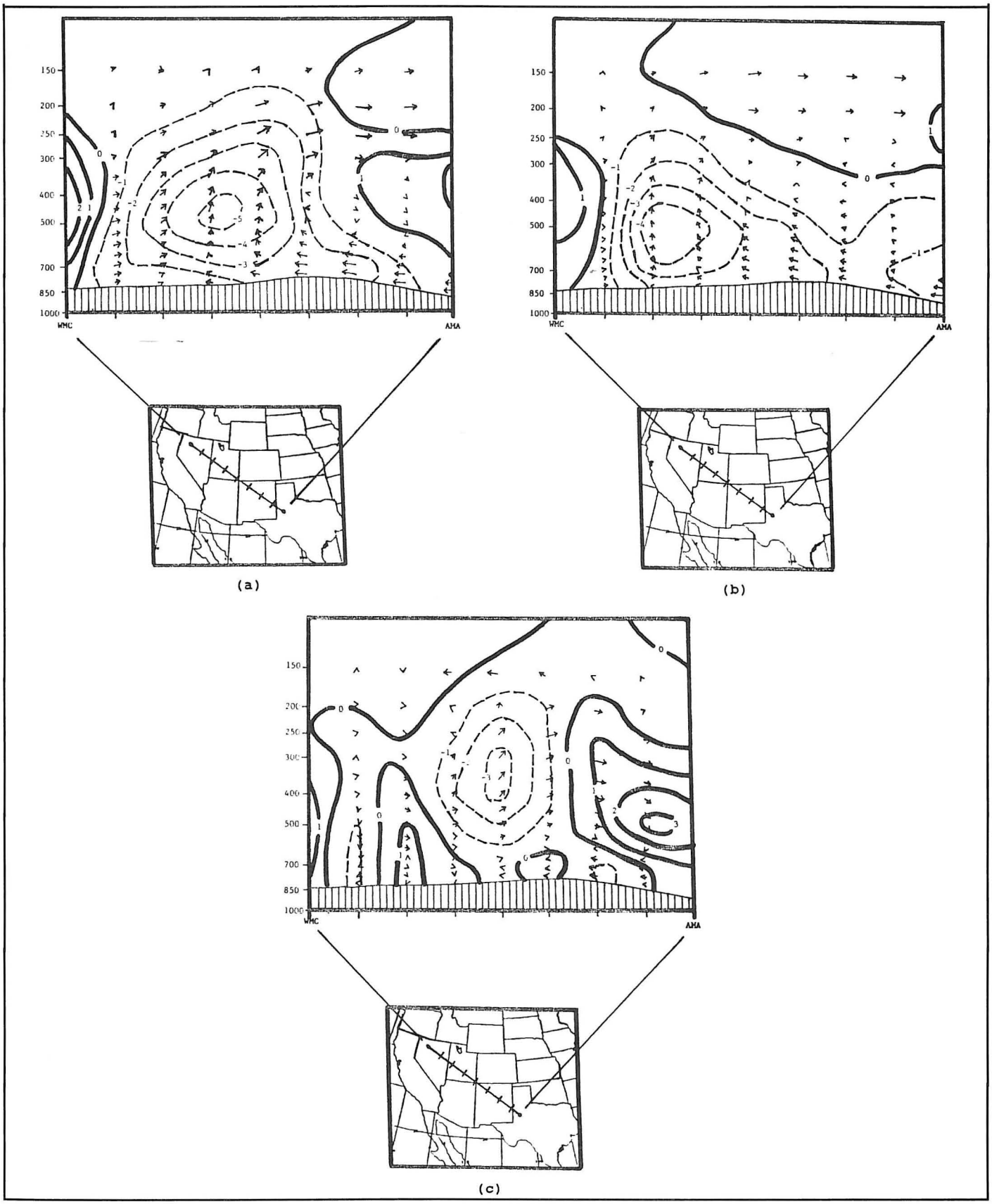

Fig. 15. Ageostrophic circulation (arrows) and omega (dashed/solid) tangent to the cross-section valid at 0000 UTC 26 October for (a) 00-hour forecast and (b) 1200 UTC 25 October, 12-hour forecast, and (c) difference fields of the ageostrophic circulation and omega (00-hour minus 12-hour forecast). Intervals of omega are $\mu b\ s^{-1}$.